Immune Regulatory Role of Parasympathetic Nervous System in Murine Corneal Allografts via Inhibition of Dendritic Cell Activation and T Cell Polarization

Dong Ihll Lee,[1] So Young Kim,[1] Yong Woo Ji,[1] Areum Yeo,[1] Jiwon Jeon,[1] Jong Suk Song,[2] and Hyung Keun Lee[1,3,4]

[1]Institute of Vision Research, Department of Ophthalmology, Yonsei University College of Medicine, Seoul, Korea
[2]Department of Ophthalmology, Korea University College of Medicine, Seoul, Korea
[3]Institute of Vascular Disease and Metabolism, Yonsei University College of Medicine, Seoul, Korea
[4]The Cornea Dystrophy Research Institute, Yonsei University College of Medicine, Seoul, Korea

Correspondence: Hyung Keun Lee, Department of Ophthalmology, Gangnam Severance Hospital, Yonsei University College of Medicine, 211 Eonjuro, Gangnam-gu, Seoul 06273, Korea; shadik@yuhs.ac.

DIL and SYK contributed equally to the work presented here and should therefore be regarded as co-first authors.

Received: May 26, 2025
Accepted: February 15, 2026
Published: March 12, 2026

Citation: Lee DI, Kim SY, Ji YW, et al. Immune regulatory role of parasympathetic nervous system in murine corneal allografts via inhibition of dendritic cell activation and T cell polarization. *Invest Ophthalmol Vis Sci.* 2026;67(3):26. https://doi.org/10.1167/iovs.67.3.26

Purpose. This study aimed to investigate the role of the parasympathetic nervous system in the allorecognition and rejection of murine corneal allografts.

Methods. We used 8- to 12-week-old male C57BL/6 (B6 and 1Ab) and BALB/C (IAd) murine models of corneal allografts. Following keratoplasty, graft survival rate and opacity were assessed for 5 weeks with or without the administration of a 0.1 mL scopolamine injection. Transcriptome changes and the presence of infiltrating antigen-presenting cells (APCs) and specific T-cell types were serially determined from the donor corneal button and draining lymph nodes (LNs) until 5 weeks after the keratoplasty procedure.

Results. Compared with the syngeneic models, the alloimmune models were observed to have significantly distinct gene expression profiles following keratoplasty. The total number of differentially expressed genes (DEGs; defined as $\geq$2-fold change) in the alloaccepted (allo-ac) models relative to the syngeneic ones was 1046 (712 upregulated and 334 downregulated), whereas 148 DEGs (136 upregulated and 12 downregulated) were identified when the Allo-ac models were compared to the allo-rejected (allo-rj) ones. Corneal opacity and rejection rates increased significantly after scopolamine injection. Flow analysis revealed significantly increased $CD11b^+$, $CD11c^+$, and $F4/80^+$ cell infiltration in the donor cornea following the scopolamine treatment. Additionally, reduced $Foxp3^+$ regulatory T (Treg) generation and enhanced Th1/Th17 polarization in the draining LNs were found in the scopolamine-treated allograft.

Conclusions. Parasympathetic innervation may play a critical role in regulating corneal allograft survival by modulating APC activation, reducing $Foxp3^+$ Treg generation, and enhancing Th1/Th17 polarization.

Keywords: parasympathetic nerves, corneal transplantation, dendritic cell, T cell, allograft rejection

Corneal transplantation is the most commonly performed form of tissue transplantation, with over 60,000 procedures conducted annually. Although robust evidence of immune privilege is well-established in rodent models, where long-term survival of fully allogeneic corneal allografts frequently exceeds 50% even in the absence of topical corticosteroids, immunologic rejection remains a leading cause of graft failure following penetrating keratoplasty (PK). This is particularly evident in high-risk patients, who constitute a substantial proportion of PK cases.[1,2] In patients undergoing PK for keratoconus, graft survival rates at 5 years can reach 90%; in contrast, individuals with pseudophakic bullous keratopathy demonstrate considerably lower 5-year survival rates—approximately 60%.[1,3] The underlying mechanisms contributing to these disparities remain incompletely understood.

The cornea is among the most densely innervated tissues in the human body.[4] Beyond their sensory functions, corneal nerves are critical for maintaining ocular surface integrity and modulating inflammation by releasing trophic factors that support epithelial homeostasis and intercellular signaling. Consequently, nerve damage due to trauma or disease may lead to diminished corneal sensation and compromised ocular surface function.[5] Acetylcholine (ACh), a well-characterized neurotransmitter in the central and peripheral nervous systems, has been reported to exert a wide range of effects beyond classical cholinergic pathways. Following its isolation from non-cholinergically innervated tissues by Dale

and Dudley,[6] ACh has been detected in a broad spectrum of mammalian cells and tissues, as well as across diverse life forms, including *eubacteria*, *archaea*, and plants.[7–9] Previous studies have demonstrated that lymphocytes contain substantial quantities of ACh,[10,11] and nicotine exposure has been shown to increase plasma ACh concentrations.[6,10] Moreover, ACh has been identified in various immune cells, including monocytes and dendritic cells (DCs).[12–14]

Recent investigations have explored the role of ACh and parasympathetic receptors in modulating alloimmune responses in solid organ transplantation.[15–18] Although research has examined the effects of corneal nerve ablation on allograft survival, relatively few studies have focused on the influence of parasympathetic innervation or its primary neurotransmitter—ACh—on corneal graft outcomes. Understanding the anatomic presence and functional contributions of specific neurotransmitter systems is essential for elucidating the neuroimmune mechanisms involved in corneal allograft survival.

Therefore, this study aimed to investigate the role of the parasympathetic nervous system in modulating alloimmune responses using a murine corneal allograft model with scopolamine injection. We focused on delineating the effects of parasympathetic neural activity on DC and T cell activation, regulatory T cell (Treg) generation, and overall graft survival.

Methods

Mice

Male BALB/c (H-2d) and C57BL/6 (H-2b) mice, aged 8 to 12 weeks, were purchased from The Jackson Laboratory (Bar Harbor, ME, USA). Mice were housed in individually ventilated cages with sawdust bedding under a 12-hour light/dark cycle. All procedures were approved by the Institutional Animal Care and Use Committee of Yonsei University College of Medicine (approval no. 3-2016-0099) and adhered to the Association for Research in Vision and Ophthalmology Statement for the Use of Animals in Ophthalmic and Vision Research.

Corneal Allograft Surgery

Orthotopic corneal transplantation was performed using standard murine protocols as previously described.[19,20] Briefly, 2.0-mm-diameter central donor corneal buttons were excised from C57BL/6 mice and sutured onto graft beds prepared by trephining a 2.0-mm site in the central cornea of BALB/c mice (allogeneic group). To control for non-alloantigenic effects of the procedure, a syngeneic group (BALB/c to BALB/c) was included. Graft clarity was evaluated via slit-lamp biomicroscopy every 3 days for the first 2 weeks, followed by weekly assessments up to 5 weeks. Grafts were considered rejected when corneal opacity prevented visualization of iris details, using a standardized grading scale (range = 0–5). This model facilitates longitudinal monitoring of graft status without requiring euthanization of the animals.

To inhibit parasympathetic activity, a subcutaneous scopolamine injection protocol commonly used in dry eye models was used. Mice in the parasympathetic inhibition group received 0.1 mL scopolamine hydrobromide (15 mg/mL; Sigma-Aldrich, St. Louis, MO, USA) subcutaneously every other day for 21 days post-transplantation, followed by 2 daily injections for an additional 2 weeks.

Tissue Preparation for Transcriptomic Analysis

For transcriptome analysis, mice were euthanized 4 weeks after transplantation surgeries, and after 5 weeks (molecular and flow works) for the collection of donor corneal buttons and draining lymph nodes (LNs). Then, the excised tissues were dissected and stored at −80°C for RNA analysis. For transcriptome analysis, the fresh excised donor buttons were snap-frozen in liquid nitrogen and pulverized to a fine powder using a pre-chilled mortar and pestle. Tissue powder was transferred into 1.5 mL tubes containing 300 µL QIAzol reagent (Qiagen, Hilden, Germany). Homogenates were vortexed for 15 seconds, shaken for 10 minutes (REAX 2000, Heidolph), and centrifuged briefly. Chloroform (60 µL) was added, and the mixture was vortexed for 15 seconds and incubated at room temperature for 3 minutes. Phase separation was achieved using phase-lock gel tubes (Heavy, 5 Prime), followed by centrifugation at 12,000 × *g* for 15 minutes. The aqueous phase was collected for RNA extraction.

RNA Extraction and Quantitative Real-Time PCR

For qPCR analysis, total RNA was extracted from the cornea and LNs using the RNeasy Micro Kit (Qiagen). The cDNA synthesis was performed with the Superscript III Kit (Invitrogen, Carlsbad, CA, USA). The qRT-PCR was carried out using SYBR Premix Ex Taq (Takara Bio, Otsu, Japan) on a StepOnePlus Real-Time PCR System (Applied Biosystems, Foster City, CA, USA). Primer sequences for *GAPDH* (Mm_001289726_m1) and muscarinic receptor subtypes *M1*, *M2*, and *M3* are listed in Table 1.

Affymetrix Whole Transcript Expression Array

Gene expression profiling was conducted according to the manufacturer's protocol (GeneChip Whole Transcript PLUS Reagent Kit, Affymetrix). Sense-strand cDNA was synthesized and fragmented, then biotin-labeled using the GeneChip WT Terminal Labeling Kit. Approximately 5.5 µg of labeled target DNA was hybridized to the Affymetrix GeneChip Mouse 2.0 ST Array at 45°C for 16 hours. Arrays were subsequently washed, stained on a GeneChip Fluidics Station 450, and scanned using a GCS3000 Scanner. Signal intensities were processed using Affymetrix GeneChip Command Console software.

Table 1. Primer Sequence for Real-Time qPCR

Gene name	Forward	Backward	Gene Bank Number
M1	GCC TAC AGC TGG AAA GAA GAA G	TGT GCC TCA GGA TCT ACC ATA G	NM001112697
M2	CAT GCA CAC CAA CAA GTA CCA	GCT GCT TGG TCA TCT TCA CAA	NM203491
M3	CCA AGC TAC CCT CCT CAG ATA A	CAG TTG TCA CGG TCA TCC ATA C	NM033269

Investigative Ophthalmology & Visual Science

Table 2. Antibodies and Fluorochromes for Flow Cytometry

Target	Conjugate	Isotype	Clone	Cat No.	Manufacturer
CD207	APC	IgG2a, κ	4C7	144205	Biolegend
CD11b	PE	IgG2b, kappa	M1/70	12-0112-82	eBioscience
CD25	PE	IgG1, lambda	PC61.5	12-0251-82	eBioscience
CD4	PE-Cy5	IgG2b, kappa	RM4-5	15-0041-82	eBioscience
	PE-Cy7	IgG2a, kappa	RM4-5	25-0042-82	
CD11c	FITC	IgG	N418	11-0114-82	eBioscience
CD3	FITC	IgG2b, kappa	17A2	11-0032-82	eBioscience
Foxp3	APC	IgG2a, kappa	FJK-16s	17-5773-82	eBioscience
CD8	Cy5.5	IgG2a, kappa	53-6.7	35-0081-82	eBioscience
IFN-γ	PE	IgG1, kappa	XMG1.2	12-7319-42	eBioscience
IL-4	APC	IgG1, kappa	11B11	17-7041-82	eBioscience
IL-17	FITC	IgG2a, kappa	eBio17B7	11-7179-42	eBioscience
F4/80$^+$	PE-Cy7	IgG2a, kappa	BM8	25-4801-82	eBioscience
Rat IgG1 kappa isotype control	PE	IgG1, kappa	eBRG1	12-4301-82	eBioscience
Rat IgG2a kappa isotype control	APC	IgG2a, kappa	eBR2a	17-4321-81	eBioscience

Microarray Data Processing and Statistical Analysis

Raw CEL files were extracted using the Affymetrix Command Console Software and normalized using the robust multi-array average algorithm in the Expression Console Software. Differentially expressed genes (DEGs) were identified via fold-change analysis between test and control groups. Hierarchical clustering was conducted using complete linkage and Euclidean distance metrics. Functional annotation and gene-enrichment analyses were performed using the DAVID bioinformatics tool (http://david.abcc.ncifcrf.gov/home.jsp). All statistical tests and data visualizations were performed using R software (version 3.1.2; www.r-project.org).

Fluorescence-Activated Cell Sorting

Fluorescence-activated cell sorting (FACS) analysis was performed as previously described.[21] Single-cell suspensions from LNs and corneal tissue were prepared using enzymatic digestion with 100 U/mL collagenase D and 15 µg/mL DNase I (Sigma-Aldrich) at 37°C for 40 minutes. For surface marker and intracellular staining, the samples were incubated with fluorochrome-conjugated monoclonal antibodies according to the manufacturer's protocols. Detailed information on antibody clones, fluorochromes, catalog numbers, and suppliers is provided in Table 2. The following antibodies were used for surface staining: FITC-conjugated anti-CD11c, FITC-conjugated anti-CD3, PE-conjugated anti-CD11b, PE-conjugated anti-CD25, PE-Cy5 or PE-Cy7-conjugated anti-CD4, PE-Cy7-conjugated anti-F4/80, and Cy5.5-conjugated anti-CD8 (all from eBioscience, San Diego, CA, USA), as well as APC-conjugated anti-CD207 (BioLegend, San Diego, CA, USA). For intracellular staining, APC-conjugated anti-Foxp3, PE-conjugated anti-IFN-γ, APC-conjugated anti-IL-4, and FITC-conjugated anti-IL-17 (all from eBioscience) were used. For intracellular cytokine detection, cells were stimulated with Phorbol 12-myristate 13-acetate (PMA) and ionomycin in the presence of brefeldin A, followed by fixation and permeabilization (eBioscience Foxp3/Transcription Factor Staining Buffer Set) according to the manufacturer's protocol. All stained samples were acquired on a FACSCanto II flow cytometer (BD Biosciences) and analyzed using FlowJo software (Tree Star). Compensation was performed for each fluorochrome, and isotype controls were used to validate gating strategies. For Treg analysis, live singlet lymphocytes were sequentially gated as CD3$^+$CD4$^+$ T cells, and CD25$^+$FoxP3$^+$ cells were defined within this CD3$^+$CD4$^+$ parent gate using isotype-matched controls to set the positive thresholds. Isotype-matched control antibodies (Rat IgG1 κ isotype control [clone eBRG1, PE, cat# 12-4301-82; eBioscience] for CD25 and Rat IgG2a κ isotype control [clone eBR2a, APC, cat# 17-4321-81, eBioscience] for FoxP3) were stained under identical conditions and applied specifically within the CD3$^+$CD4$^+$ T cell population to establish positivity thresholds. Compensation was verified using UltraComp eBeads (ThermoFisher Scientific). Data are presented as representative pseudocolor dot plots and quantified as a percentage of positive cells within relevant gates.

Statistical Analysis

Chi-square tests were used to compare categorical data, including corneal opacity scores. Kaplan–Meier survival curves were generated for graft rejection analysis and compared using the log rank test. Continuous variables were assessed for normality using the Shapiro–Wilk test. Normally distributed data were expressed as mean ± standard deviation and compared using independent two-sample *t*-tests, paired *t*-tests, or 1-way analysis of variance. The homogeneity of variance was tested using Levene's test. Post hoc comparisons were corrected using the Bonferroni method. A two-sided P value < 0.05 was considered statistically significant. All statistical analyses were performed using SAS (version 9.4; SAS Institute, Cary, NC, USA) and SPSS (version 25.0; IBM, Armonk, NY, USA).

Results

Corneal Transcriptomic Alterations Under Syngeneic and Allogeneic Transplantation Conditions

To assess transcriptomic differences, total mRNA expression profiles were compared between syngeneic and allogeneic graft conditions. High correlation coefficients (Pearson's $R > 0.913$, $P < 0.001$) confirmed data robustness. Hierarchical clustering revealed markedly distinct gene expression profiles between syngeneic and allograft

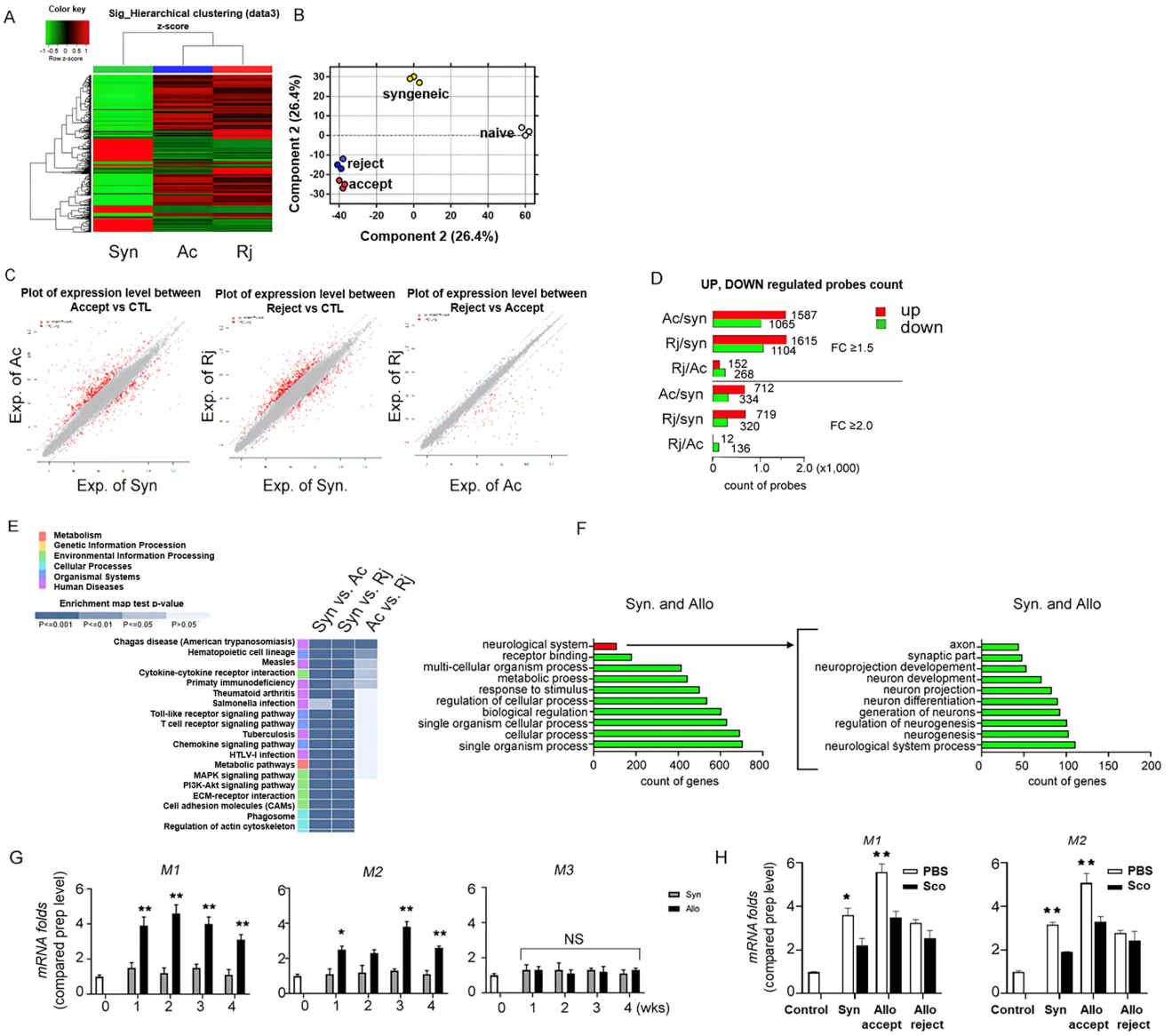

Figure 1. Comparative transcriptomic profiling of syngeneic and allogeneic corneal grafts. (**A**) Representative images and hierarchical heatmap of corneas from syngeneic (Syn), allograft-accepting (Ac), and rejecting (Rj) groups. Three independent experiments were conducted, each with three corneas. Mice were euthanized on postoperative day 35. (**B**) Multidimensional scaling (MDS) plot of differentially expressed genes (DEGs) among naïve, syngeneic, allograft-accepting, and rejecting corneas. (**C**) Scatter plots comparing DEGs across syngeneic, Ac, and Rj groups. The data represent pooled results from three independent experiments. (**D**) Histograms showing the number of upregulated (*red*) and downregulated (*green*) genes. The *upper* and *lower panels* represent DEGs with fold changes (FC) $\geq$ 1.5 and $\geq$ 2.0, respectively. (**E, F**) Pathway analyses using the Kyoto Encyclopedia of Genes and Genomes (KEGG) **E** and Gene Ontology (GO) **F** databases (statistical significance set at $P < 0.05$). Subanalyses of genes related to the neurological system are represented as histograms (*right*). (**G**) Quantitative real-time PCR (qRT-PCR) analysis of muscarinic receptor subtypes M1, M2, and M3 mRNA expression in syngeneic and allogeneic corneas over time. Data are from two independent experiments (3 corneal buttons per group; $^{**}P < 0.01$, $^{*}P < 0.05$. (**H**) The qRT-PCR analysis of muscarinic receptor subtypes M1 and M2 mRNA expression in mouse corneal tissue across experimental groups. Experimental groups include control, syngeneic grafts, allogeneic accept and reject, each with and without scopolamine (Sco) treatment. Bar graphs display fold changes of M1 (*left*) and M2 (*right*) mRNA normalized to control (mean $\pm$ SEM). Data are from two independent experiments (3 corneal buttons per group). $^{**}P < 0.01$, $^{*}P < 0.05$.

groups at 5 weeks post-transplantation (Fig. 1A). Transcriptomic comparisons between accepted and rejected allografts demonstrated similar gene expression patterns despite phenotypic differences in corneal transparency and neovascularization (see Figs. 1A, 1B). Multidimensional scaling analysis corroborated the proximity of transcriptomes between accepted and rejected allografts. Conversely, comparison among clear corneas, namely, naïve, syngeneic, and accepted allografts (allo-ac), revealed distinct transcriptomic signatures. DEGs across syngeneic, allo-ac, and rejected allograft (allo-rj) groups are summarized in Supplementary Datafile S1. Allo-ac corneas exhibited a higher number of activated genes than those of syngeneic and Allo-rj groups (Figs. 1C, 1D). The total number of DEGs ($\geq$2-fold change) in allo-ac relative to syngeneic was 1046 (712 upregulated and 334 downregu-

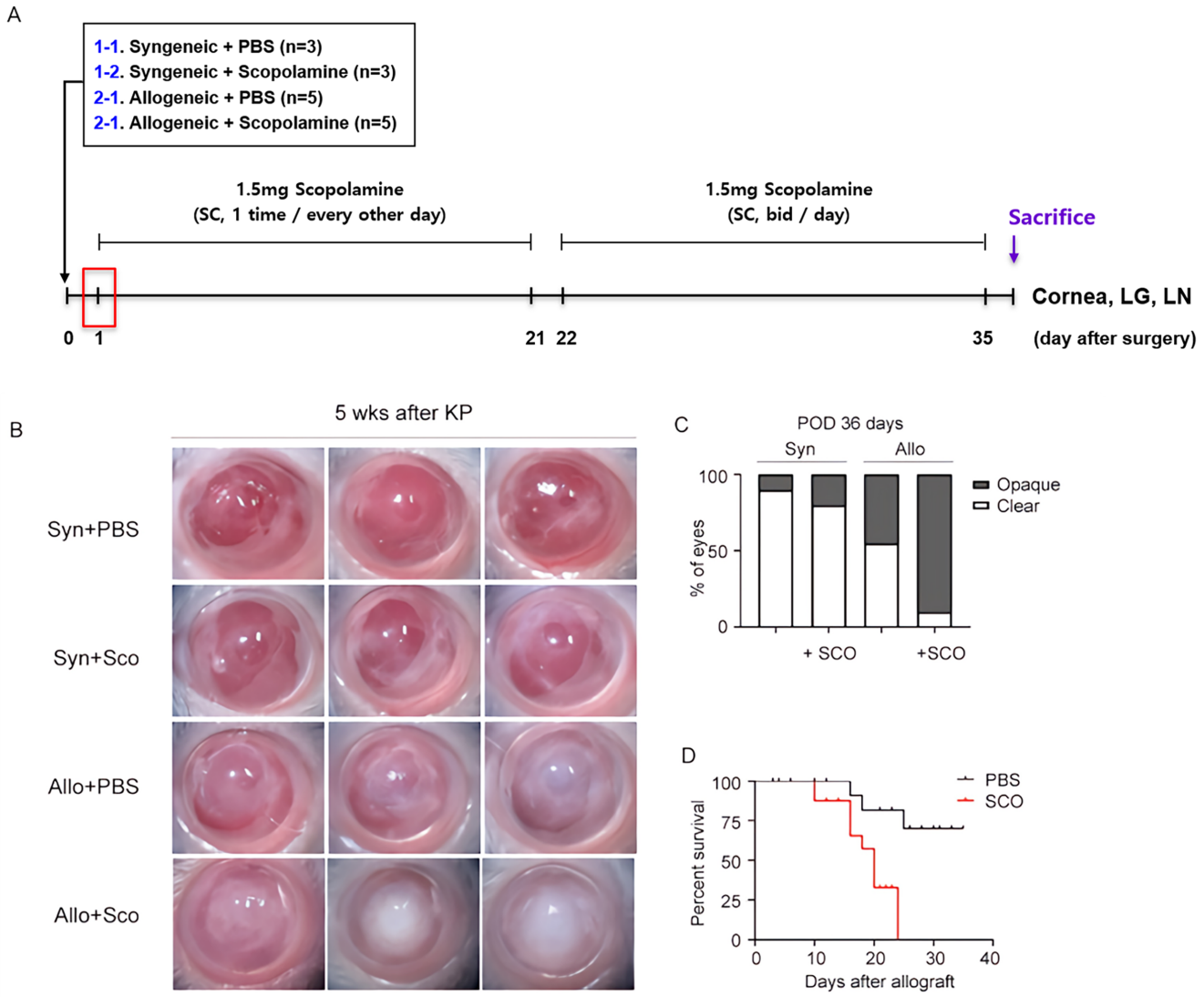

Figure 2. Evaluation of graft survival and corneal opacity following scopolamine administration. (A) Schematic of the keratoplasty procedure and scopolamine injection timeline. **(B)** Representative images of corneas from each treatment group: Syn-PBS (syngeneic graft with PBS), Syn-Sco (syngeneic graft with scopolamine, 0.1%, 0.1 mL), Allo-PBS (allogeneic graft with PBS), and Allo-Sco (allogeneic graft with scopolamine). **(C)** Assessment of corneal clarity on postoperative day (POD) 35 using a standardized grading scale (see Methods). Corneal clarity was significantly reduced in the Allo-Sco group ($P < 0.001$). **(D)** Kaplan–Meier survival curves for corneal grafts. *Black*: PBS-treated (sham) and *Red*: scopolamine-treated.

lated), whereas 148 DEGs (12 upregulated and 136 downregulated) were identified when comparing allo-ac with allo-rj.

Pathway analysis using Kyoto Encyclopedia of Genes and Genomes (KEGG) and Gene Ontology (GO) databases was performed to identify activated gene networks. KEGG pathway analysis revealed significant differences between syngeneic and allograft conditions in pathways related to primary immunodeficiency, toll-like receptor signaling, and T cell receptor signaling. Comparisons between allo-ac and allo-rj revealed enrichment in Chagas disease, hematopoietic cell lineage, and rheumatoid arthritis-related pathways (Fig. 1E). GO enrichment analysis identified the top 10 biological processes, with neuron-related pathways ranking highly (Fig. 1F; $P = 1.268 \times 10^{-158}$, Bonferroni-adjusted). Among these, 55 axon-associated and 78 neuron projection-associated genes were identified. Fewer than 15 neuron-related genes significantly differed between the allo-ac and allo-rj groups ($P < 0.001$), with notable changes observed in muscarinic (M) receptor gene expression under allograft conditions. Because mice possess only three M receptor subtypes (in contrast to 5 in humans),[22–24] we quantified expression levels of *M1*, *M2*, and *M3* subtypes. *M1* and *M2* mRNA levels were elevated in allografted corneas compared with syngeneic controls (Fig. 1G). Quantitative qPCR analysis revealed distinct patterns of muscarinic ACh receptor subtype mRNA expression in the mouse cornea following transplantation and scopolamine intervention. As shown in Figure 1H, both *M1* and *M2* mRNA levels were significantly elevated in allogeneic accept groups compared to control and syngeneic groups. Notably, the upregulation observed in the accept group

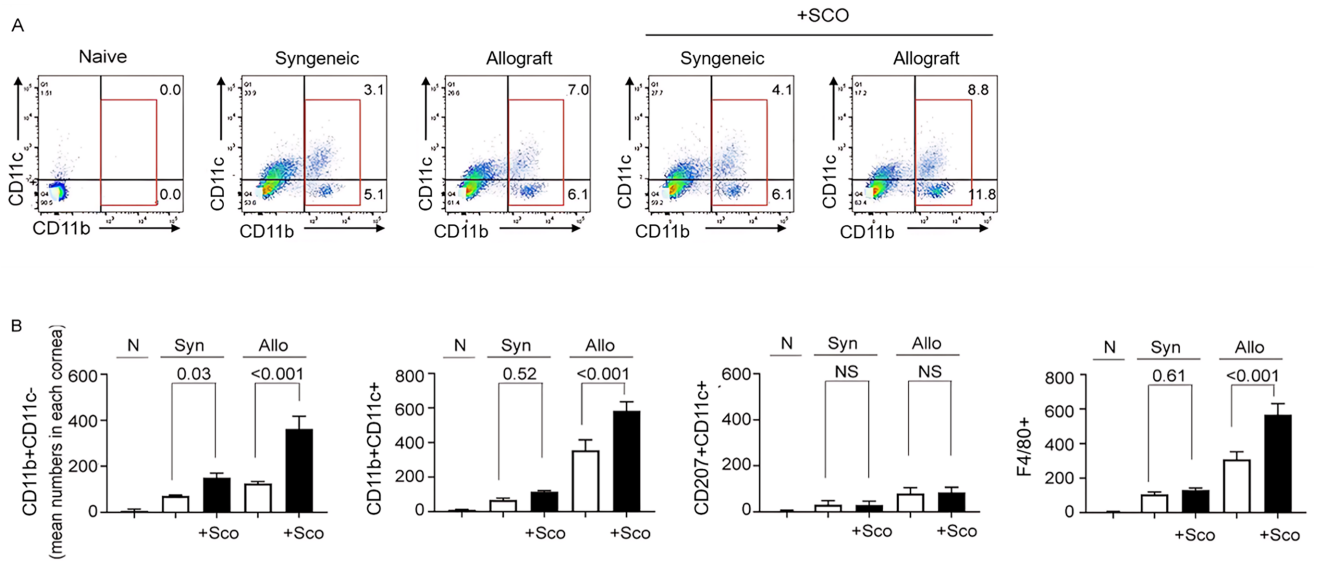

Figure 3. Effect of scopolamine injection on dendritic cell infiltration in transplanted cornea. (**A**) Representative flow cytometry plots of donor cornea buttons at 5 weeks post-transplantation. (**B**) Quantification of $CD11b^+$, $CD11c^+$, and $F4/80^+$ cells in donor corneal buttons at 5 weeks. Data represent mean ± standard deviation (SD; from ≥3 independent experiments).

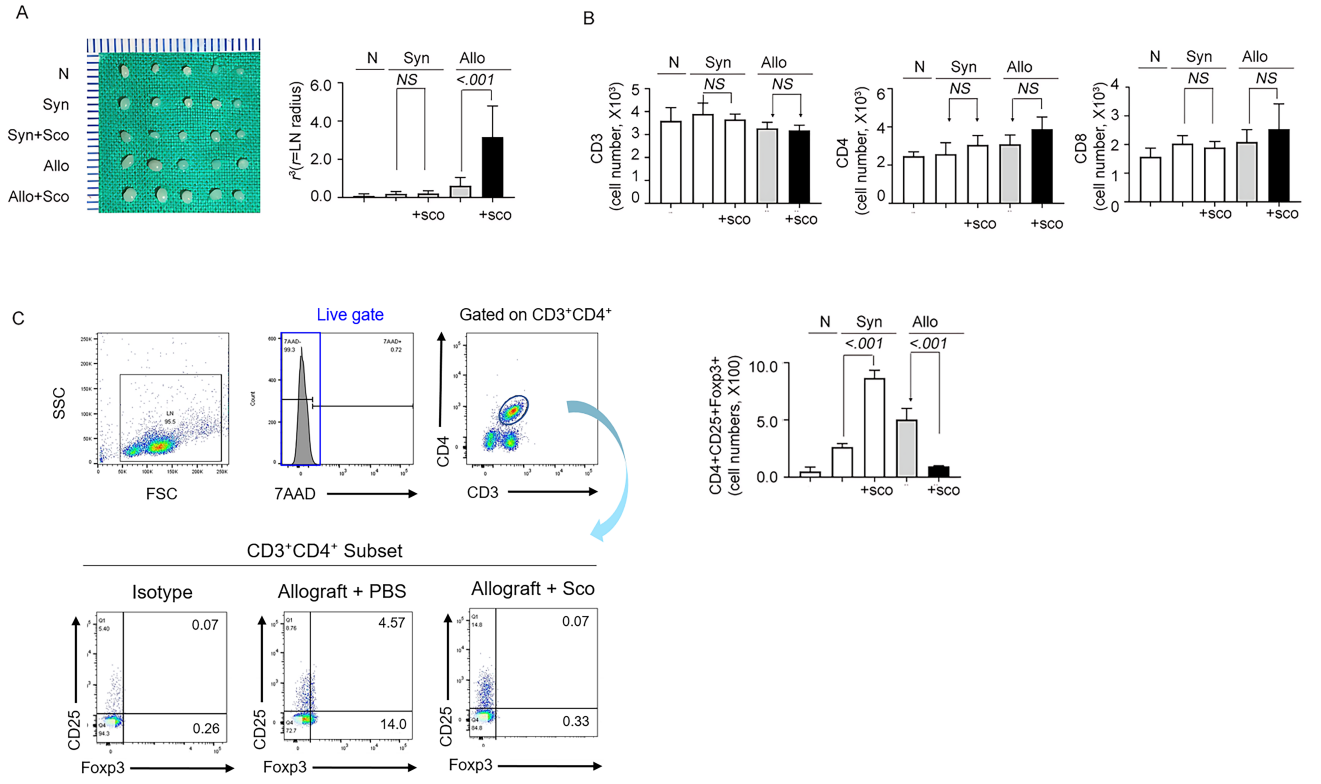

Figure 4. Analysis of draining lymph node (LN) changes and T cell populations following scopolamine treatment. (**A**) Representative images (*left*) and quantification (*right*) of LN volume at 5 weeks post-keratoplasty. NS, not significant. (**B**) Histogram of $CD3^+$, $CD4^+$, and $CD8^+$ T cell counts in donor corneal tissue at 5 weeks (mean ± standard deviation [SD]; ≥3 independent experiments). (**C**) Representative flow cytometry gating strategy (*left*) and quantification (*right*) of $CD25^+FoxP3^+$ regulatory T cells (Tregs) in draining lymph nodes 5 weeks post-keratoplasty. Live lymphocytes were sequentially gated: FSC/SSC → singlets → 7-AAD^- live cells → $CD3^+$ → $CD3^+CD4^+$ T cells. Isotype-matched control antibodies were applied specifically to the $CD3^+CD4^+$ parent population to set positive thresholds for CD25 and FoxP3 staining. One-way ANOVA with Bonferroni post-hoc test; mean ± SD; $n = 3$ to 5 per group.

Investigative Ophthalmology & Visual Science

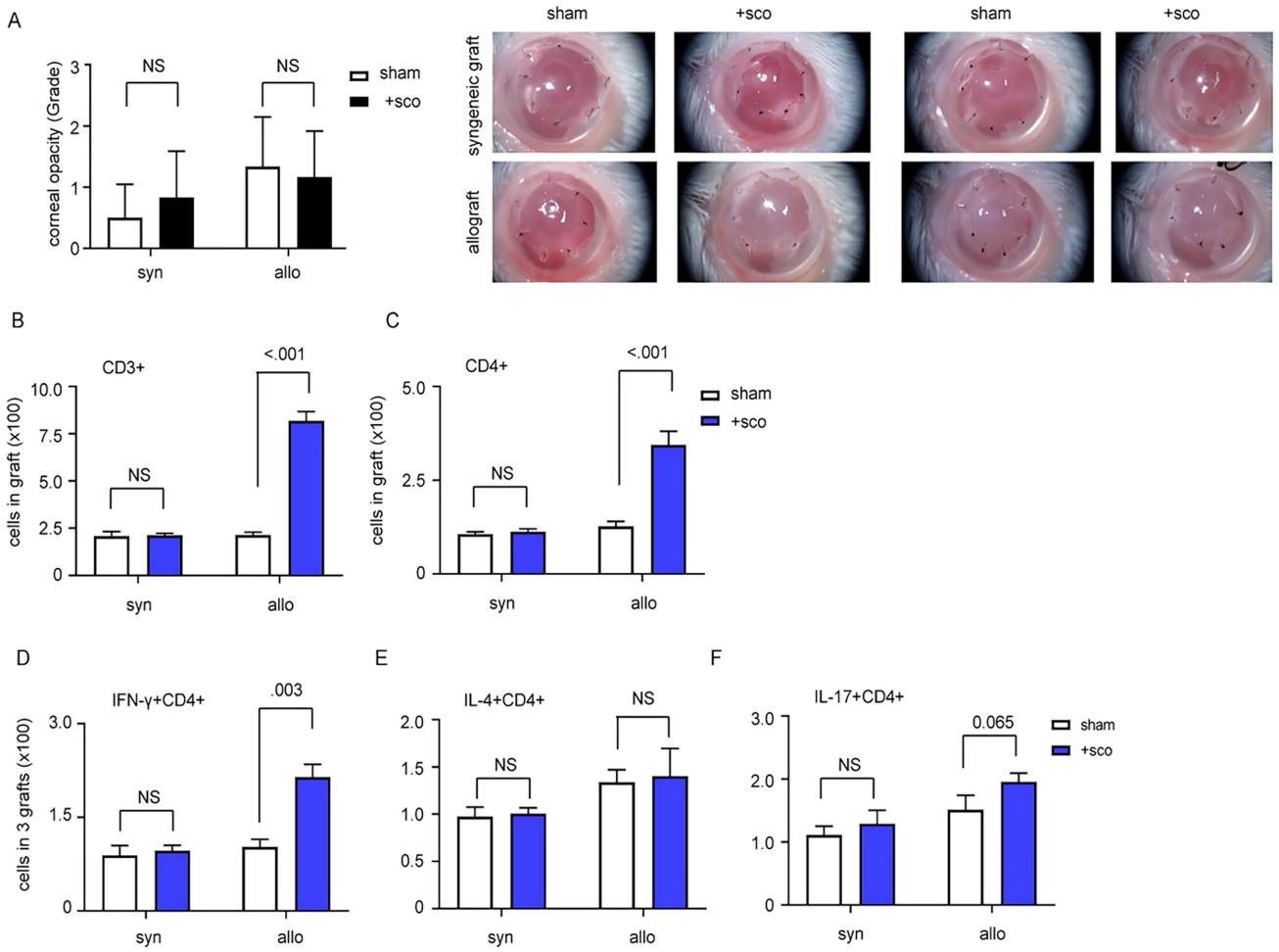

Figure 5. Impact of scopolamine on corneal clarity and T cell infiltration in allografts. (**A**) Corneal opacity scores and representative images at 5 weeks post-transplantation. Grading was performed in a blinded manner by a single investigator ($n = 5$, mean ± standard deviation [SD]). (**B, C**) Flow cytometry analysis of graft-infiltrating $CD3^+$ **B** and $CD4^+$ **C** T cells at 5 weeks. (**D**) Quantification of Th1, Th2, and Th17 cell subsets in the corneal graft at 5 weeks post-transplantation. Data in panels **B** to **D** represent the mean ± SD from three independent experiments.

was markedly diminished after scopolamine administration (see Fig. 1H).

Blocking Parasympathetic Innervation Accelerates Graft Rejection and Increases DC Infiltration

To investigate the functional relevance of M receptor upregulation, we used systemic chemical denervation using scopolamine, a broad-spectrum M receptor antagonist, in a murine allograft model (Fig. 2A). Scopolamine administration did not significantly affect graft survival in syngeneic transplants (Figs. 2B, 2C). However, in the allograft group, corneal opacity markedly increased, and complete graft rejection occurred within 25 days post-keratoplasty (see Figs. 2C, 2D). As DC activation is a key initiating step in alloimmunity, we evaluated DC subpopulations. In both syngeneic and allogeneic grafts, $CD11b^+CD11c^-$, $CD11b^+CD11c^+$, and $CD11c^+CD207^+$ DCs were elevated relative to naïve controls (Figs. 3A, 3B). These DC subsets were significantly more abundant in the allograft group at 5 weeks post-transplantation ($P = 0.002$ for $CD11b^+CD11c^-$, $P < 0.001$ for $CD11b^+CD11c^+$, $P = 0.009$ for $CD11c^+CD207^+$). Classical DCs ($CD11c^+CD11b^+$) in allografts were 2.3-fold higher than in syngeneic corneas, whereas $CD11b^+CD11c^-$ DCs increased 1.3-fold. $F4/80^+$ cells were elevated in both transplant types; however, scopolamine did not alter their frequency in syngeneic grafts. In contrast, allograft recipients treated with scopolamine showed a 4.3-fold increase in $F4/80^+$ cells compared to the syngeneic scopolamine group. $CD207^+$ DC frequency was slightly higher in allografts but did not significantly change with scopolamine administration (see Fig. 3B).

Scopolamine Suppresses Treg Generation and Migration Post-Transplantation

Analysis of draining LNs revealed that scopolamine treatment in allografted mice significantly increased LN size and volume by 3.9-fold relative to PBS-treated controls at 5 weeks post-transplantation (Fig. 4A). However, total T cell populations ($CD3^+$, $CD4^+$, and $CD8^+$) in draining

LNs remained unchanged (Fig. 4B). In syngeneic grafts, Foxp3$^+$CD25$^+$ Tregs were elevated regardless of treatment. Similarly, Tregs were increased in untreated allografts. Strikingly, scopolamine-treated allograft recipients exhibited an almost complete loss of Foxp3$^+$CD25$^+$ Tregs (<1% of CD4$^+$ cells) in draining LNs (Fig. 4C), and no Tregs were detected in corneal or conjunctival tissues (data not shown).

Scopolamine Promotes Th1/Th17 Polarization in Early Graft Response

To assess early immune responses, corneal allografts were examined 10 days post-surgery, prior to suture removal. Corneal transparency was comparable between scopolamine- and PBS-treated groups at this time point (Fig. 5A). Nevertheless, CD3$^+$ and CD4$^+$ T cell infiltration was significantly increased in scopolamine-treated allografts ($P < 0.001$; Fig. 5B). The mean number of CD3$^+$ cells in allografts rose from 211 ± 31 to 799 ± 102 ($P < 0.001$) following scopolamine administration. Whereas syngeneic grafts showed no significant changes in CD3$^+$ cell numbers, scopolamine significantly elevated CD4$^+$CD3$^+$ T cells in allografted corneas ($P < 0.001$; Fig. 5C). To further characterize the CD4$^+$ T cell response, intracellular cytokine analysis was performed using flow cytometry and qPCR. Scopolamine-treated allografts exhibited a marked increase in IFN-γ^+CD4$^+$ T cells compared to IL-4$^+$ or IL-17$^+$ subsets (Figs. 5D–F). In syngeneic grafts, scopolamine did not significantly alter IFN-γ^+CD4$^+$ T cell numbers. However, in allografts, scopolamine led to a 2.2-fold increase in IFN-γ^+CD4$^+$ T cells compared with those in PBS-treated controls (see Fig. 5D). By contrast, IL-4$^+$ and IL-17$^+$ CD4$^+$ T cells were significantly fewer and unaffected by treatment.

Discussion

Despite the high success rate of corneal transplantation without systemic immunosuppression or major histocompatibility complex (MHC) matching, graft rejection remains a significant concern, particularly in high-risk recipients such as those with denervated neurotrophic keratitis. This study offers novel insights into the mechanisms underlying graft survival and rejection. First, transcriptomic comparisons between accepted and rejected allografts revealed striking similarities despite marked phenotypic differences in graft clarity and vascularity. Second, parasympathetic innervation was critical for Treg generation in draining LNs and modulating ocular surface inflammation.

Transcriptomic Profiles of Accepted Versus Rejected Allografts

Transcriptomic analyses revealed considerable similarity between accepted and rejected allografts, despite their differing phenotypes—transparent and opaque. Furthermore, transcriptomes from naïve, syngeneic, and accepted allografts differed markedly despite exhibiting clear corneas. Although the precise significance of these findings remains unclear, they suggest that different molecular mechanisms may underlie corneal clarity in each condition rather than a singular, shared pathway. Although the exact nature of this transcriptome similarity could not be elucidated in this study, the close resemblance between the transcriptomes of accepted and rejected allografts may imply that, with appropriate regulation of key genes or pathways, a rejected graft may be capable of reverting toward a state of immune acceptance.

Several DEGs were identified in rejected grafts, including *CCL3*, *IL1B*, *TRAPPC3* (trafficking protein particle complex subunit 3), and *VTE3* (a methyltransferase), with high statistical significance ($P = 3.83 \times 10^{-60}$). KEGG pathway analysis revealed significant enrichment in cytokine–cytokine receptor interactions, hematopoiesis, MAPK signaling, TNF signaling, and metabolic pathways (see Fig. 1). The number of activated genes was higher in accepted allografts than in rejected ones (339 vs. 208 DEGs). This indicates that the accepted grafts are not simply in a quiescent state but are actively engaging in immune regulation and expressing effective genes for maintaining clarity, which may differentiate them from the naïve or syngeneic clear corneas at the transcriptomic level.

Role of Innervation in Maintaining Immune Privilege

Although studies investigating the role of corneal innervation in allograft immunity are limited, Niederkorn et al. have demonstrated that corneal trephination disrupts anterior chamber-associated immune deviation (ACAID) and increases graft rejection.[25–27] Other evidence supports the critical role of neural regulation in maintaining ACAID.[28,29]

Trephination of the contralateral (but not the ipsilateral) eye increased the rejection rate,[26,30] suggesting that immune privilege is not solely dependent on localized ocular mechanisms but involves systemic neuroimmune interactions, which might be mediated by a neural network. To further investigate this, we used an M receptor antagonist—scopolamine—to specifically disrupt parasympathetic signaling. Interestingly, this intervention significantly increased donor cornea opacity and graft rejection rate with infiltrating CD11b$^+$CD11c$^+$ in donor cornea buttons (see Figs. 2, 3). Both tissue-resident and circulating immune cells can produce ACh and express its receptors.[6,10,24] Under allograft conditions, ACh content and receptor expression were elevated in peripheral blood mononuclear cells.[6,31] The role of the cholinergic system in graft survival has been examined in skin,[16,32] kidney,[15,16] and lung[17,33] allografts, where cholinergic deficiency consistently correlated with increased rejection and organ dysfunction. These findings suggest that parasympathetic signaling plays a regulatory role in corneal graft survival. In addition to the cholinergic system, other neurotransmitters, such as substance P, have been implicated in allograft rejection.[25] Our results support the hypothesis that corneal nerves, particularly cholinergic fibers, contribute to maintaining corneal clarity and play an immunoregulatory role in graft tolerance. Different neurotransmitter systems may influence the activation states of DCs, cytokine production, and effector cell (e.g. T and B cell) activity, thereby shaping graft outcomes.

Following scopolamine injection, frequencies of CD11c$^+$ and F4/80$^+$ cells increased in draining LNs of allograft recipients. However, the population of CD207$^+$CD11c$^+$ Langerhans cells (LCs), defined as Langerin$^+$CD11c$^+$MHCII$^+$ cells residing within the intraepithelial layer,[34,35] was not affected by M blockade. We assessed the frequency of these triple-positive DCs in both ocular tissues and draining LNs under syngeneic and allogeneic conditions but observed

Investigative Ophthalmology & Visual Science

no increase in LC migration or activation in the allograft context. Morphologically distinct from skin LCs,[34] ocular LCs are embedded within deeper epithelial layers and are separated from the tear film by tight junctions; this may limit their ability to sample or present antigens. Nonetheless, ocular LCs have been associated with corneal nerve regeneration[36] and lymphangiogenesis.[37] To clarify their role in graft rejection, future studies using CD207-conditional knockout mice are warranted. Because donor-derived LCs are transferred with the graft tissue, their precise function in initiating or modulating alloimmune responses must be further examined, despite their limited abundance.

Parasympathetic Regulation of Tregs and Implications for Graft Survival

A particularly notable observation was the marked reduction of Tregs following scopolamine treatment from the early keratoplastic period. Given the central role of T cells in graft rejection, we assessed T cell subsets and cytokine profiles in draining LNs and found Foxp3$^+$ Tregs to be markedly reduced in the presence of parasympathetic blockade. Although the precise mechanism remains to be elucidated, this reduction is consistent with an anti-inflammatory role of cholinergic signaling in supporting regulatory pathways. However, it does not in itself distinguish among altered Treg proliferation, survival, or trafficking. Accordingly, our data do not provide direct evidence for a compensatory proliferative expansion of Tregs in response to parasympathetic blockade, and such mechanisms remain speculative until dedicated proliferation and functional assays are performed in future studies. Cholinergic sensory neurons can detect cytokines and damage-associated molecular patterns, which leads to norepinephrine release from the celiac ganglion and activation of T cells to produce ACh in the spleen.[38] ACh suppresses the release of pro-inflammatory cytokines such as TNF-α[13] and IL-1β.[39] In dry eye models, systemic muscarinic AChR blockade has been shown to alter Treg function and the balance between effector and regulatory CD4 T-cell responses, without markedly changing Treg frequencies.[40] Together with our findings, these data support a broader role of parasympathetic signaling in shaping the balance between regulatory and effector responses, rather than indicating a uniform proliferative effect on Tregs in all settings. Moreover, DCs and T cells notoriously express muscarinic receptors[24] and have regulatory functions in various pathologic conditions.[6,13] Therefore, ACh may directly suppress DCs and alloimmunity T cell activation. In the present study, disruption of parasympathetic signaling was associated with marked alterations in DC activation and T-cell balance, and these changes may underlie the observed effects on graft outcome, although the precise mechanisms will require further investigation.

The flow cytometric analyses revealed an unexpectedly high frequency of CD25$^-$FoxP3$^+$ cells within the draining LNs in our transplantation models. CD25$^-$FoxP3$^+$ cells are generally regarded as non-suppressive or transient FoxP3-expressing cells, rather than bona fide Tregs with stable suppressive function.[41] Therefore, the increased frequency of CD25$^-$FoxP3$^+$ cells in allograft recipients may reflect ongoing inflammation or the presence of unstable Treg subsets, rather than effective regulatory activity. Consistent with established transplantation literature, our primary analyses focused on the CD25$^+$FoxP3$^+$ subset, which is considered the canonical Treg population critical for immune regulation and graft survival.[42] However, further studies may be needed to clarify the origin, stability, and functional relevance of CD25$^-$FoxP3$^+$ cells and their potential role in alloimmune regulation.

This study has some limitations. First, systemic administration of an M receptor antagonist might block parasympathetic signaling incompletely, particularly at the ocular surface. Additionally, both M and nicotinic receptors are expressed in ocular tissues,[23,41] and future studies should aim to target both receptor types to fully evaluate parasympathetic contributions. Second, M receptor subtype expression differs between mice and humans,[23] limiting direct translatability of these findings to clinical settings. In conclusion, our findings demonstrate that parasympathetic innervation plays a critical role in regulating corneal allograft survival, largely by modulating cytokine expression, antigen-presenting cell activation, LN trafficking, and CD8$^+$ T cell infiltration. These results may explain the poor graft prognosis observed in denervated ocular environments.

Given the potential roles of other neural signaling systems, such as substance P, dopamine, and sympathetic innervation, in ocular immune regulation, future studies should explore these networks in the context of corneal transplantation.

Acknowledgments

Supported by the Advanced Science Research Program (Grant no. RS-2024-00344204) through the National Research Foundation of Korea (NRF), funded by the Ministry of Education, Science, and Technology, Seoul, Korea. The funders had no role in this study.

Disclosure: **D.I. Lee**, None; **S.Y. Kim**, None; **Y.W. Ji**, None; **A. Yeo**, None; **J. Jeon**, None; **J.S. Song**, None; **H.K. Lee**, None

References

1. Shimazaki J, Den S, Omoto M, Satake Y, Shimmura S, Tsubota K. Prospective, randomized study of the efficacy of systemic cyclosporine in high-risk corneal transplantation. *Am JOphthalmol*. Jul 2011;152(1):33–39.e31.
2. [No authors listed.] Report of the organ transplant panel. Corneal transplantation. Council on scientific affairs. *JAMA*. 1988;259(5):719–722.
3. Niederkorn JY. High-risk corneal allografts and why they lose their immune privilege. *Curr Opin Allergy Clin Immunol*. 2010;10(5):493–497.
4. Muller LJ, Marfurt CF, Kruse F, Tervo TM. Corneal nerves: structure, contents and function. *Exp Eye Res*. 2003;76(5):521–542.
5. Marfurt CF, Cox J, Deek S, Dvorscak L. Anatomy of the human corneal innervation. *Exp Eye Res*. 2010;90(4):478–492.
6. Fujii T, Mashimo M, Moriwaki Y, et al. Expression and function of the cholinergic system in immune cells. *Front Immunol*. 2017;8:1085.
7. Grando SA, Kist DA, Qi M, Dahl MV. Human keratinocytes synthesize, secrete, and degrade acetylcholine. *Allergy*. 1993;101(1):32–36.
8. Horiuchi Y, Kimura R, Kato N, et al. Evolutional study on acetylcholine expression. *Life Sci*. 2003;72(15):1745–1756.
9. Yamada T, Fujii T, Kanai T, et al. Expression of acetylcholine (ACh) and ACh-synthesizing activity in Archaea. *Life Sci*. 2005;77(16):1935–1944.

10. Fujii T, Yamada S, Yamaguchi N, Fujimoto K, Suzuki T, Kawashima K. Species differences in the concentration of acetylcholine, a neurotransmitter, in whole blood and plasma. *Neurosci Lett*. 1995;201(3):207–210.
11. Filippini P, Cesario A, Fini M, Locatelli F, Rutella S. The Yin and Yang of non-neuronal alpha7-nicotinic receptors in inflammation and autoimmunity. *Semin Immunopathol*. 2012;13(5):644–655.
12. Gori S, Vermeulen M, Remes-Lenicov F, et al. Acetylcholine polarizes dendritic cells toward a Th2-promoting profile. *Allergy*. 2017;72(2):221–231.
13. Salamone G, Lombardi G, Gori S, et al. Cholinergic modulation of dendritic cell function. *J Neuroimmunol*. 2011;236(1-2):47–56.
14. Reardon C, Duncan GS, Brustle A, et al. Lymphocyte-derived ACh regulates local innate but not adaptive immunity. *Proc Natl Acad Sci USA*. 2013;110(4):1410–1415.
15. Meixner M, Atanasova S, Padberg W, Grau V. Expression of acetylcholine receptors by experimental rat renal allografts. *Biomed Res Int*. 2014;2014:289656.
16. Sadis C, Detienne S, Vokaer B, et al. The cholinergic anti-inflammatory pathway delays TLR-induced skin allograft rejection in mice: cholinergic pathway modulates alloreactivity. *Biomed Res Int*. 2013;8(11):e79984.
17. Hirschburger M, Zakrzewicz A, Kummer W, Padberg W, Grau V. Nicotine attenuates macrophage infiltration in rat lung allografts. *J Heart Lung Transplant*. 2009;28(5):493–500.
18. Methe H, Zimmer E, Grimm C, Nabauer M, Koglin J. Evidence for a role of toll-like receptor 4 in development of chronic allograft rejection after cardiac transplantation. *Transplantation*. 2004;78(9):1324–1331.
19. Liu Y, Hamrah P, Zhang Q, Taylor AW, Dana MR. Draining lymph nodes of corneal transplant hosts exhibit evidence for donor major histocompatibility complex (MHC) class II-positive dendritic cells derived from MHC class II-negative grafts. *J Exp Med*. 2002;195(2):259–268.
20. Chauhan SK, Saban DR, Lee HK, Dana R. Levels of Foxp3 in regulatory T cells reflect their functional status in transplantation. *J Immunol*. 2009;182(1):148–153.
21. Seo Y, Ji YW, Lee SM, et al. Activation of HIF-1α (hypoxia inducible factor-1α) prevents dry eye-induced acinar cell death in the lacrimal gland. *Cell Death Dis*. 2014;5:e1309.
22. Grueb M, Reinthal E, Rohrbach JM, Bartz-Schmidt KU. Muscarinic acetylcholine receptor subtypes in human corneal epithelium and endothelium. *Graefes Arch Clin Exp Ophthalmol*. 2006;244(9):1191–1195.
23. Liu S, Li J, Tan DT, Beuerman RW. Expression and function of muscarinic receptor subtypes on human cornea and conjunctiva. *Invest Ophthalmol Vis Sci*. 2007;48(7):2987–2996.
24. Kawashima K, Yoshikawa K, Fujii YX, Moriwaki Y, Misawa H. Expression and function of genes encoding cholinergic components in murine immune cells. *Life Sci*. 2007;80(24-25):2314–2319.
25. Mo J, Neelam S, Mellon J, Brown JR, Niederkorn JY. Effect of corneal nerve ablation on immune tolerance induced by corneal allografts, oral immunization, or anterior chamber injection of antigens. *Invest Ophthalmol Vis Sci*. 2017;58(1):137–148.
26. Paunicka KJ, Mellon J, Robertson D, Petroll M, Brown JR, Niederkorn JY. Severing corneal nerves in one eye induces sympathetic loss of immune privilege and promotes rejection of future corneal allografts placed in either eye. *Am J Transplant*. 2015;15(6):1490–1501.
27. Niederkorn JY. Immunology of corneal allografts: insights from animal models. *J Clin Exp Ophthalmol*. 2015;6(3):429.
28. Li X, Taylor S, Zegarelli B, Shen S, O'Rourke J, Cone RE. The induction of splenic suppressor T cells through an immune-privileged site requires an intact sympathetic nervous system. *J Neuroimmunol*. 2004;153(1-2):40–49.
29. Streilein JW, Bradley D, Sano Y, Sonoda Y. Immunosuppressive properties of tissues obtained from eyes with experimentally manipulated corneas. *Invest Ophthalmol Vis Sci*. 1996;37(2):413–424.
30. Neelam S, Mellon J, Wilkerson A, Niederkorn JY. Induction of contrasuppressor cells and loss of immune privilege produced by corneal nerve ablation. *Invest Ophthalmol Vis Sci*. 2018;59(11):4738–4747.
31. Hecker A, Mikulski Z, Lips KS, et al. Pivotal Advance: Up-regulation of acetylcholine synthesis and paracrine cholinergic signaling in intravascular transplant leukocytes during rejection of rat renal allografts. *J Leukoc Biol*. 2009;86(1):13–22.
32. De Rosa MJ, Dionisio L, Agriello E, Bouzat C, Esandi Mdel C. Alpha 7 nicotinic acetylcholine receptor modulates lymphocyte activation. *Life Sci*. 2009;85(11-12):444–449.
33. Biallas S, Wilker S, Lips KS, et al. Immunohistochemical detection of nicotinic acetylcholine receptor subunits alpha9 and alpha10 in rat lung isografts and allografts. *Life Sci*. 2007;80(24-25):2286–2289.
34. Hattori T, Chauhan SK, Lee H, et al. Characterization of Langerin-expressing dendritic cell subsets in the normal cornea. *Invest Ophthalmol Vis Sci*. 2011;52(7):4598–4604.
35. Hattori T, Takahashi H, Dana R. Novel insights into the immunoregulatory function and localization of dendritic cells. *Cornea*. 2016;35(1):S49–S54.
36. Choi EY, Kang HG, Lee CH, et al. Langerhans cells prevent subbasal nerve damage and upregulate neurotrophic factors in dry eye disease. *PLoS One*. 2017;12(4):e0176153.
37. Ji YW, Lee JL, Kang HG, et al. Corneal lymphangiogenesis facilitates ocular surface inflammation and cell trafficking in dry eye disease. *The Ocul Surf*. 2018;16(3):306–313.
38. Andersson U, Tracey KJ. Neural reflexes in inflammation and immunity. *J Exp Med*. 2012;209(6):1057–1068.
39. Rynko AE, Fryer AD, Jacoby DB. Interleukin-1beta mediates virus-induced m2 muscarinic receptor dysfunction and airway hyperreactivity. *Am J Respir Cell Mol Biol*. 2014;51(4):494–501.
40. Chen Y, Chauhan SK, Lee HS, et al. Effect of desiccating environmental stress versus systemic muscarinic AChR blockade on dry eye immunopathogenesis. *Invest Ophthalmol Vis Sci*. 2013;54(4):2457–2464.
41. Wang J, Ioan-Facsinay A, van der Voort EI, Huizinga TW, Toes RE. Transient expression of FOXP3 in human activated nonregulatory CD4+ T cells. *Eur J Immunol*. 2007;37(1):129–138.
42. Kang SM, Tang Q, Bluestone JA. CD4+CD25+ regulatory T cells in transplantation: progress, challenges and prospects. *Am J Transplant*. 2007;7(6):1457–1463.

Investigative Ophthalmology & Visual Science